Microstructures of magnetic tunneling junctions

Lai-feng Li
Technical Institute of Physics and Chemistry, Chinese Academy of Sciences, Beijing, China

Xiaoyong Liu[a] and Gang Xiao
Department of Physics, Brown University, Providence, Rhode Island 02912

We have investigated the microstructures of magnetic tunneling junctions using high-resolution transmission electron microscopy (HRTEM). These junctions exhibit large magnetoresistance of 34% at room temperature and at tens of gauss. HRTEM reveals well-defined layered polycrystalline metallic structures. The important Al_2O_3 tunneling barrier has an amorphous structure containing a few tiny crystalline inhomogeneties. Though the barrier is flat over large length scales, its interfaces with the neighboring electrodes are rough. We have characterized the roughness amplitude and wavelength, which are consistent with the magnitude of offset bias fields in measured hysteretic magnetoresistance curves. © *2003 American Institute of Physics.* [DOI: 10.1063/1.1528312]

I. INTRODUCTION

There has been considerable interest in magnetic tunnel-junctions (MTJs), [1–3] due to their potential technological applications in nonvolatile magnetic random access memory (MRAM) and as a generation of magnetic sensors. The tunneling of MTJ devices depends on the relative orientations of magnetization vectors between the top and bottom ferromagnetic (FM) layers separated by an oxide tunnel barrier. Much effort has been made in optimizing sample fabrication parameters for enhancing the magnetoresistance (MR) ratio while keeping junction resistance-area product to a minimum. [4,5] The creation of a stoichoimetric, pin-hole free, and smooth barrier is likely to be a prerequisite to the attainment of large MR and other beneficial properties. A number of techniques have been utilized to characterize barrier structures, such as Rutherford backscattering spectrometry and *in situ* resistance *I–V* characterization. Of these, high-resolution transmission electron microscopy (HRTEM) is one of the best tools for extracting MTJ microstructures and growth mechanisms at the atomic level. To date, there have been very few studies[6–8] of MTJs using HRTEM. In this article, we report our microstructure analysis of Al_2O_3 barrier based MTJs with large MR ratios using HRTEM. Particular attention is paid to the tunnel barrier structure. The extracted barrier roughness profiles generate an interlayer Néel coupling field that is in agreement with experimentally observed magnetic bias fields.

II. EXPERIMENTAL DETAIL

Our MTJ samples are multilayers with the structure Pt (30 nm)|Py (3 nm)| FeMn (13 nm)|Py (6 nm)|Al_2O_3|Py (12 nm)|Al (49 nm), grown at room temperature using dc magnetron sputtering. The Si(100) substrates were thermally oxidized prior to deposition. All layers were deposited in a 120 Oe applied field, which defines the easy-axis direction of the ferromagnetic layers. The seed layer consisting of Py($Fe_{81}Ni_{19}$) is used to promote the (111) texture growth of the antiferromagnetic FeMn layer, which exchange biases the magnetization vector of the bottom electrode, Py (6 nm). The Al_2O_3 barrier was formed by exposing a thin layer of Al (1–2 nm) to an oxygen plasma. The oxidation time was optimized to maximize MR. The top electrode, Py (12 nm), serves as the free magnetic layer, whose magnetization vector is relatively free to respond to external magnetic fields. The magnetization direction of the pinned layer was reinforced by annealing the sample at 170°C in dc field of 1.6 kG for 3 min following deposition. A self-aligned optical lithography process was used to pattern the junctions for the four-point resistance measurement. The junctions used in this study were rectangular shape and had area 100×150 μm^2.

The samples used for the cross-sectional TEM imaging were prepared by cutting MTJs into two small pieces, gluing them face to face, and finally grinding and polishing them down to a thickness of ~ 25 μm. A subsequent ion-beam thinning process was used to make the sample electron transparent. A thin carbon layer was coated on the sample surface before loading into the microscope chamber. HRTEM investigations were carried out in a JEOL 2010FEG microscope working at 200 kV with a point resolution of 0.19 nm. Before taking TEM images, we also did x-ray diffraction characterization on selected samples with a Simens x-ray diffractometer (D5000) using monochromatic Cu K_α radiation source with step width of 0.01°.

III. RESULTS AND DISCUSSIONS

Figure 1(a) shows a representative cross-sectional TEM micrograph of an as-deposited MTJ structure. After a moderate annealing at 170°C, there are marked improvements in the microstructure of the same sample. Figure 1(b) shows a TEM micrograph of the annealed sample. Although the Py/FeMn/Py layers underneath the Al_2O_3 barrier are not easily resolvable due to relatively small difference in atomic mass, and therefore diffraction contrast, between FeMn (Z
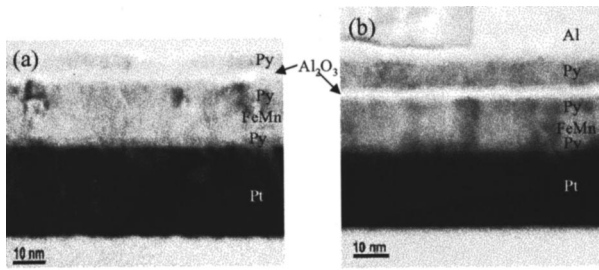
a)Electronic mail: xiaoyong_liu@brown.edu

FIG. 1. Cross-sectional TEM images of our magnetic tunneling junctions. (a) As-deposited sample and (b) postannealed sample.

FIG. 3. Magnetoresistance curve of a typical postannealed MTJ. Within the field range shown, only the magnetization of the free electrode is allowed to switch. The MR curve is shifted by −3.5 Oe due to Néel coupling.

=25.5) and Py ($Z=27.7$), each layer is visible with well-defined and flat interfaces. The layer thicknesses agree well with predetermined values. It is also noted that, on both sides of the barrier layer, the grains grow with a columnar structure, oriented with the long axis in the growth direction. The average diameter of the columns is 8 nm. It should be emphasized that the TEM photographs shown in this article are examples highly representative of our extensive investigations.

The MTJ structure was further examined using x-ray diffraction. As shown in Fig. 2, the FeMn (111) peak after annealing is more prominent, demonstrating a significant (111) texture improvement, which is preferable for producing higher exchange bias fields for the pinned Py layer. The obvious separation between (111) peaks for FeMn and Py ($2\theta=43.5°$ and $44.2°$, respectively) implies that the layers are highly textured. From the symmetric scan of the FeMn (111) peak, we were able to estimate the grain size of FeMn by using Scherrer's equation.[9] The results are 84.8 and 86.3 Å for the annealed and as-deposited samples, respectively, which agree with the TEM observations. Our results support the argument that enhanced exchange bias upon thermal annealing is mainly due to an improved (111) texture, and not due to changes in grain size.[10]

Figure 3 shows the magnetoresistance curve of an annealed MTJ sample. The external magnetic field sweeps along the easy axis of the junction. The sweeping range (~40 Oe) is far below the exchange bias field for the pinned layer (~400 Oe), so that only the switching behavior of top
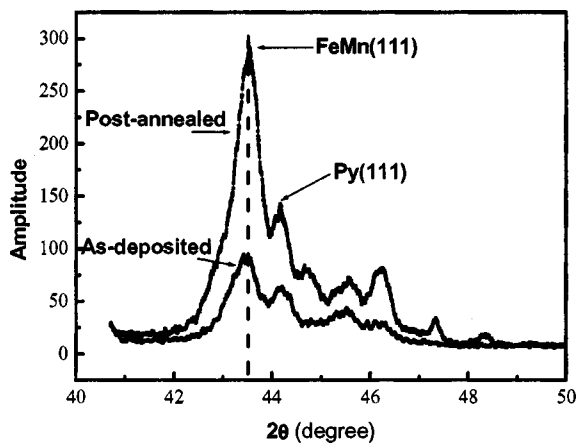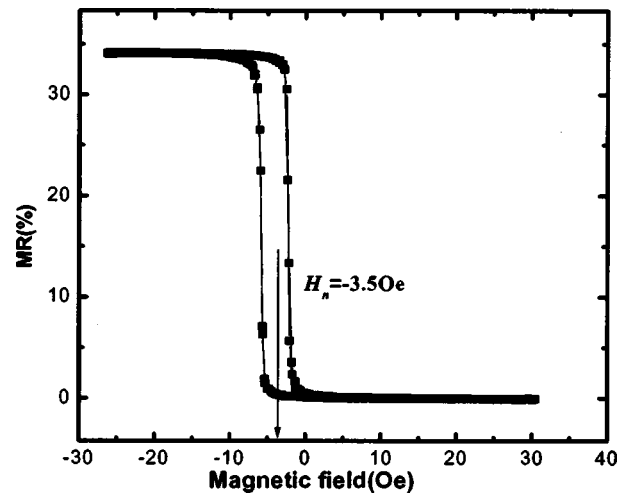
free layer is observed. A clean, square hysteresis loop is observed in the MR curve, indicating nearly perfect parallel (P) and antiparallel (AP) magnetization configurations between the top and bottom Py layers outside the switching region. A MR ratio of 34% is consistently obtained. For the 30 junctions we measured, the $P\rightarrow$AP and AP$\rightarrow P$ switching fields are stable at −5.5 and −1.5 Oe, respectively, giving an average offset about −3.5Oe, this offset is caused by interlayer coupling resulting from the roughness of the barrier layer, an issue we will discuss later.

Although Fig. 1 reveals some structural information about the MTJ layer structure, HRTEM can reveal detailed interface structures, grain growth mechanisms, roughness and interfaces between layers, as well as crystal defects at the atomic scale. Figure 4 shows a representative cross-sectional HRTEM image of an MTJ sample. It can be seen that the Al_2O_3 barrier layer is of a continuous amorphous phase with an average thickness of 2.19 nm, which agrees with the numerical fit to the $I-V$ curve of the MTJ using Simmons' formula.[11] The uniformity of the barrier is one of

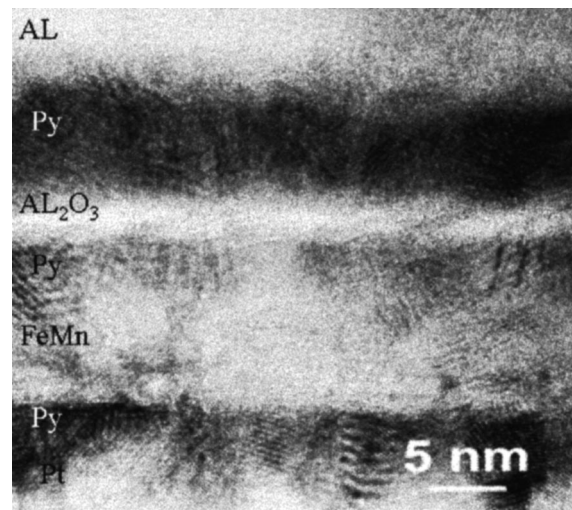FIG. 2. X-ray diffraction spectra for the junctions before and after postannealing.

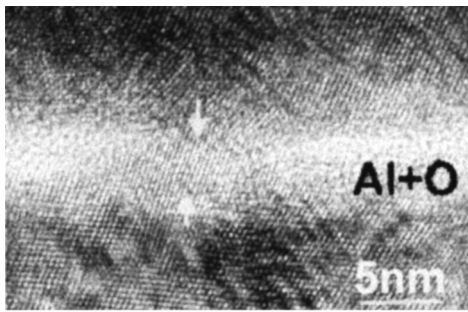FIG. 4. Cross-sectional HRTEM image of the MTJ layer structure.

FIG. 5. HRTEM micrograph of small crystalline inhomogenetics in the barrier region of a MTJ.

the reasons behind the large MR values observed in our junctions. Thickness fluctuations in the barrier and a long-range waviness are apparent in Fig. 4. It can also be seen from Fig. 4 that the Py, FeMn, and Pt layers are made of polycrystalline grains with a grain size of 8–10 nm. Continuous lattice fringes are clearly observed in each grain. In addition to lattice fringes, some Moire fringes are also observable due to the overlap of different grains in the observation direction.

Due to their negative effects on tunneling, we searched for inhomogenetics in the barrier regions. Although in most observations we found no traces of inhomogenetics in the barrier, on one occasion a small crystalline region with a length of about 5 nm has been observed, and is denoted by arrows in Fig. 5.

Microstructural details of the layer structure can be further explored via a higher resolution micrograph, shown in Fig. 6, of the Pt/Py/FeMn interfacial region. Some prominent grains have been labeled as a, b, and c. Between grains a and b, there is a twin boundary marked by the arrows in Fig. 6 Grain b and c are oriented close to a common $\langle 110 \rangle$ zone axis. The linkage between grain a and the FeMn layer is also oriented to a $\langle 110 \rangle$ zone axis with an ordered transition. Although there are some small discrepancies in orientation, it is clear that all of the layers except Al_2O_3 are almost totally crystalline and textured, as confirmed by Fourier transform pattern (shown in inset of Fig. 6). From the earlier analysis,
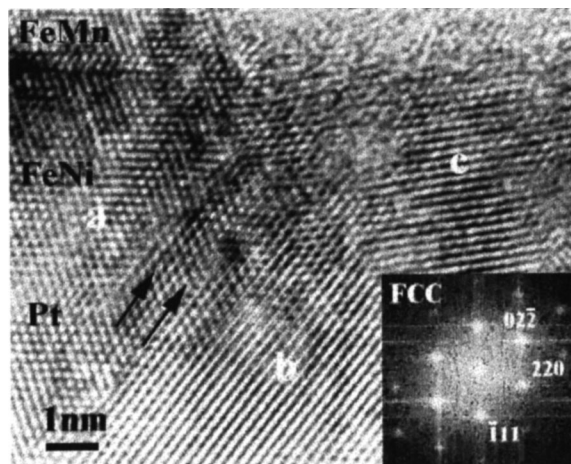

FIG. 6. A HRTEM image showing the local structure of the FeMn, Py, and Pt layers, with its Fourier transform shown in the inset.
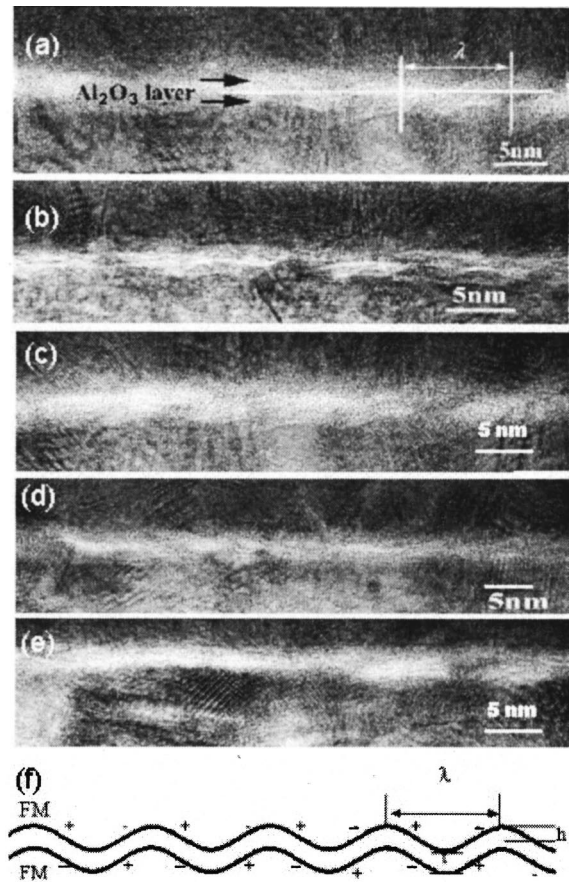

FIG. 7. (a)–(e) HRTEM images focused on the barrier layer; (f) schematic view of the roughness profile of the barrier used for analysis of Néel coupling between the FM layers.

there may exist a tendency toward (111) texture in the Pt/Py/FeMn structure, which is probably important for obtaining large exchange bias and high magnetoresistance.

As shown in Fig. 3, the free layer MR hysteresis loop is centered at a small negative offset field. This offset is due to magnetic coupling between the free and the pinned FM layers. There are two kinds of magnetic coupling existing in MTJ devices: magnetostatic coupling due to uncompensated poles at the edges of the FM layers and Néel "orange-peel" coupling due to interfacial roughness at the two barrier interfaces.[12] For the junctions we examined, the area of the junction is large, making the polar magnetostatic coupling negligible; therefore the offset of the MR loop is primarily due to the Néel coupling field in the free layer is given by [12]

$$H_N = \frac{\pi^2 h^2}{\sqrt{2}\lambda t_f} M_p e^{-2\pi\sqrt{2}t/\lambda} , \tag{1}$$

where h and λ are the amplitude and wavelength of the roughness profile of the barrier, respectively, t is the average thickness of the barrier, and M_p is the magnetization of bottom pinned Py layer.

Figures 7(a)–(e) are some representative HRTEM images focused on the barrier layer. A long-range waviness can clearly be seen. In order to accurately get the amplitude and wavelength of the roughness profile that is schematically
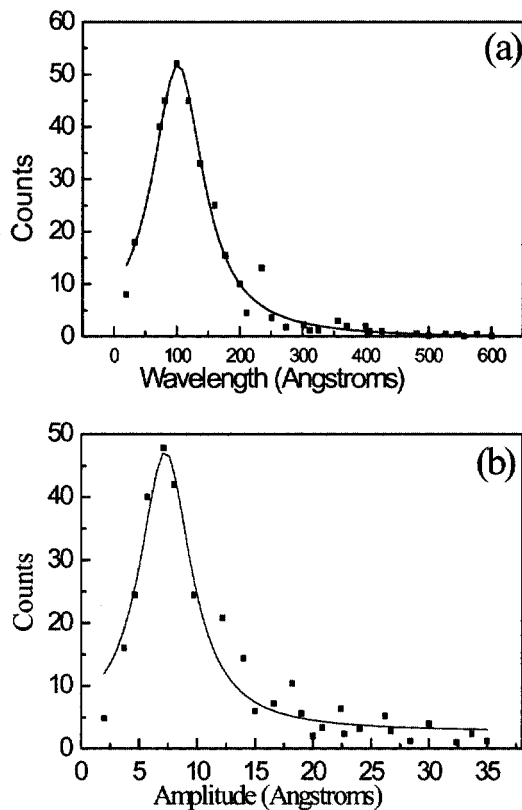
FIG. 8. Histograms of the fitted (a) wavelengths and (b) amplitudes of the roughness profile obtained from the HRTEM images.

shown in Fig. 7(f), we digitized the HRTEM images and obtained distributions of h and λ as follows.[13] First, the digitized data points relating the barrier interface as a function of the horizontal distance of barrier were picked up and smoothed. Second, the coordinates of all local adjacent maxima and minima were then recorded. Last, the effective wavelength and amplitude corresponding to each pair of points according to Fig. 7(f) were then extracted and plotted in histograms. Figure 8 shows the distributions of wavelengths and amplitudes of barrier roughness profile on many HRETM observations according to the earlier method. Both distributions basically follow a log-normal pattern, with the peak of h at 0.75 nm and λ at 10 nm. Using Néel coupling

field, H_n, to be 3.9 Oe. This result is consistent with the offset field of 3.5 Oe obtained in the MR hysteresis curve shown in Fig. 3. The small discrepancy is attributed to the finite size of the field increment (~ 0.25 Oe) used in acquiring the magnetoresistance curves and problems with the assumption of a single sinusoidal roughness profile in Néel's model.

IV. CONCLUSIONS

In summary, the microstructures of magnetic tunneling junctions have been investigated by HRTEM. The tunnel barrier is found to be amorphous and contains few weak links. High-resolution images of metallic layers on both sides of the barrier reveal well-defined polycrystalline structures with a (111) texture. These junctions exhibit a large magnetoresistance of 34% at room temperature and in a small applied field (<20 Oe). Based on the waviness of the barrier, we have calculated the theoretical Néel coupling field, which is found to be consistent with the offset bias fields calculated from magnetoresistance curves.

ACKNOWLEDGMENTS

[1] J. S. Moodera, L. R. Kinder, T. M. Wong, and R. Resurvey, Phys. Rev. Lett. **74**, 3273 (1995).
[2] S. S. P. Parkin *et al.*, J. Appl. Phys. **85**, 5828 (1999).
[3] S. Tehrani *et al.*, IEEE. Trans. Magn. **55**, 2814 (2000).
[4] J. J. Sun *et al.*, Appl. Phys. Lett. **76**, 2424 (2000).
[5] D. Song, J. Nowark, and M. Corington, J. Appl. Phys. **87**, 5179 (2000).
[6] J. S. Bae, K. H. Shin, T. D. Lee, and H. M. Lee, Appl. Phys. Lett. **80**, 1168 (2002).
[7] J. Wang, P. P. Freitas, E. Snoeck, P. Wei, and J. C. Soares, Appl. Phys. Lett. **79**, 4387 (2001).
[8] T. E. Clark, F. B. Mancoff, S. X. Wang, B. M. Clemens, and R. Sinclair, IEEE. Trans. Magn. **35**, 2922 (1999).
[9] B. E. Warren, *X-ray Diffraction* (Dover, New York, 1969), p. 253.
[10] H. Li, P. P. Freitas, Z. Wang, J. B. Sousa, P. Gogol, and J. Chapman, J. Appl. Phys. **89**, 6904 (2001).
[11] J. C. Simmons, J. Appl. Phys. **34**, 1793 (1963).
[12] L. Néel, C. R. Acad. Sci. III **255**, 1676 (1962).
[13] B. Schrag *et al.*, Appl. Phys. Lett. **77**, 2373 (2000).